Spring 2018

Modeling Crevice Corrosion of Nickel Alloy 625 in Seawater

Linsey Grzeschik
lng14@zips.uakron.edu

ABSTRACT

In this work, COMSOL Multiphysics was used to model crevice corrosion of Nickel Alloy 625 in seawater. Initial model parameters included a bulk solution of 0.6M (Cl^-) ASTM D1141-98 artificial seawater, a crevice length of 12.7mm, and applied current of $0.44V_{SHE}$. A crevice gap of 7μm and 10μm were compared using a 3.0m polarization curve of the simulated critical crevice solution for Alloy 625. A constant crevice gap of 10μm was used to compare varying polarization curves of 3.0m, 3.5m, and deaerated seawater. The model found a variation in free chloride concentration from the bulk to 1.29M (deaerated seawater polarization) and to 4.47M (3.5m polarization) at the tip of the crevice. Modeled data of species concentration, current density, and potential versus position in the crevice confirmed the effects of a smaller crevice gap and higher current density on the IR drop within the crevice. By lowering the potential from the passive region ($0.44V_{SHE}$) to the active region on the polarization curve, crevice corrosion propagation was observed in the model.

EXECUTIVE SUMMARY

Problem Statement

Crevice corrosion is a detrimental damage mechanism to alloys that are otherwise immune in the bulk environment. Crevice propagation models for alloys are limited based on experimental peak current densities from polarizations run in bulk environments. Nickel Alloy 625 is generally immune to corrosion in chloride containing environments, but it has been seen in the field and experimentally that the alloy can suffer catastrophic damage from crevice corrosion in chloride containing environments such as seawater. This occurs because the solution that develops inside the crevice (critical crevice solution) is more aggressive than the bulk. COMSOL Multiphysics was used to model the transport of species (cations, Cl^-, etc.) inside the crevice to better understand the development of the critical crevice solution (CCS). Thus, a better understanding of crevice propagation is gained through the modeling of species concentration, current density, and potential along the length of the crevice of Alloy 625 in seawater.

Summary of Results

Crevice corrosion models were run using a variety of polarization data, such as 3.0m and 3.5m critical crevice solution simulants and deaerated seawater, as surface boundary conditions for a bulk solution of ASTM D1141-98 artificial seawater (0.6M Cl^-). Bulk reactions in the model included twelve equilibrium reactions for water, nickel, iron, chromium, and their respectively formed chloride and hydroxide compounds. Two cases were compared in this report: varying crevice gap size and varying polarization curves. It should be noted that the equilibrium constants for $FeCl^+$ and $FeCl_2(s)$ were manually altered by 10^{-4} to achieve model convergence.

Varying crevice gap size resulted in an IR drop of 46mV for a 10μm gap and a drop of 56mV for a 7μm gap using the 3.0m polarization curve with an $E_{app} = 0.44V_{SHE}$. Free chloride within the crevice was 1.77M for the 7μm gap and 1.57M for the 10μm gap. Varying the polarization curves to either 3.0m, 3.5m, or deaerated seawater were modeled with a constant gap of 10μm and $E_{app} = 0.44V_{SHE.}$ The IR drop for 3.0m and deaerated seawater was comparable at 46mV, but an IR drop of 346mV was observed for the 3.5m polarization curve. Free chloride was 1.57M for the 3.0m polarization, 4.74M for the 3.5m polarization, and 1.29M for the deaerated seawater polarization.

Conclusions

IR drop for varying the crevice gap from 10μm to 7μm moved the electrode potential of the surface inside the crevice closer to the active region of dissolution on the 3.0m polarization curve, but did not bring either case into the region of active corrosion. Results were similar for the 3.0m and deaerated seawater curves with a 10μm gap in that neither IR drop resulted in placement within the active dissolution region on the respective polarization curves. However, the IR drop associated with the 3.5m polarization shifted the crevice potential at the tip of the crevice into the region of active dissolution on the polarization curve. This drop into the active region of dissolution on the polarization curve resulted in the higher concentration of both free and total chloride.

Implications

The COMSOL model sheds new light on the crevice environment so that corrosion propagation can be understood within the context of the concentration of species within the crevice. In addition, the model also allows assessment of the role of IR drop in crevice propagation. The model in its present state can provide insight into the propagation of crevice corrosion for Alloy 625 in ASTM D1141-98 artificial seawater.

This honors project has solidified my ability to run standard corrosion tests such as polarization curves. It has also enhanced my technical understanding of crevice corrosion and allowed me to develop my computer modeling capabilities. It is now possible for me to confidently manipulate various differential equations to accurately model a crevice environment and understand many cases of previous, related work in literature. Communicating these results in a comprehensive report is preparing me for a career of writing similar reports on corrosion failures and investigations. The effect of corrosion damage is abundantly apparent from the 2016 NACE *IMPACT* study as 2.7% of the US GDP is spent on corrosion damage [12]. As well, in 2017, 2% of Ohio's workforce was employed by jobs directly related to corrosion prevention and monitoring [15]. This project is an essential building block to the understanding of crevice corrosion.

Recommendations

Additional modeling will be required to understand the model's limitations surrounding the ferrous chloride equilibrium reactions. By systematically removing reactions and adding them incrementally back to the model, it may be possible to eliminate the cause of inconsistent electroneutrality along the length of the crevice. As well, running models with smaller crevice gaps and higher molality simulated critical crevice solution polarization curves will give more insight into the behavior of crevice propagation based on crevice geometry, IR drop, and critical crevice solution. The goal of inputting experimental current versus position (in the crevice) data into the model, can only be achieved if the model accurately converges and electroneutrality is maintained consistently instead of for a limited number of cases.

INTRODUCTION

The purpose of this project was to model crevice corrosion of Nickel Alloy 625 (20-23 wt% Cr, 8-10 wt% Mo, 3-4 wt% Nb, balance Ni) in seawater using COMSOL Multiphysics, a mathematical model solver and simulator. Crevice corrosion is defined as the localized attack on a metal surface at, or immediately adjacent to, a gap or crevice between two joining surfaces. The breakdown of a passive film can lead to rapid and possibly catastrophic corrosion damage. Crevice corrosion is a concern not only at metal-to-metal interfaces, but also metal-to-nonmetal interfaces. Specifically, aircraft and transportation industries combat this form of corrosion at the millions of bolt, washer, and skin material connections on planes and ships. Crevice corrosion proves to be significantly concerning in industries that operate in chloride containing environments such as seawater due to the aggressive nature of the chloride ion and associated metal chlorides within the crevice itself.

Alloy 625 is chosen for its resistance to pitting from chlorides and uniform corrosion. However, it has been observed both experimentally and in the field that Alloy 625 suffers from crevice corrosion in seawater. Species concentration in the bulk solution versus the crevice solution is drastically varied and can prove detrimental to otherwise immune alloys. By modeling the species concentrations in the crevice based on experimental critical crevice solution (CCS) parameters, the scientific community will have a better understanding of the chemistry possible within crevices.

BACKGROUND

Oldfield and Sutton describe a three stage model of crevice corrosion: depletion of oxygen within a crevice, pH fall within a crevice, and breakdown and the onset of rapid

corrosion [1, 2]. The key parameters for these stages are the composition of the alloy, bulk solution, and crevice geometry. Oldfield and Sutton further discuss the importance of the critical crevice solution (CCS). Crevice corrosion of Alloy 625 has been further modeled by Shaw, Moran, and Gartland using a model for IR and IR* in the crevice gap [3]. All of these parameters are necessary for consideration in modeling crevice corrosion of Alloy 625 in seawater.

Previous work by Dr. Diana Muñoz-Miller [4] was used as boundary conditions for the COMSOL model, with the expansion of previous model capabilities to incorporate various polarization curves. Further experimental development includes polarization curves for Alloy 625 in deaerated ASTM D1141-98 artificial seawater (DASW). Experimental measurements from the deaerated polarization curves were added to the simulation to understand the role of peak current density required for active crevice propagation. Because of the number of reactions occurring within the model, it was necessary to verify the electroneutrality of the CCS.

The corrosion module within COMSOL solves partial differential equations such as variations of the Nernst-Planck equation and Fick's 2nd Law in order to simulate potential, current, and species concentration along the length of the crevice in question. The low peak current densities in the experimental polarization curves, caused the limits of model convergence to be reached.

EXPERIMENTAL METHODS

Polarization curves of Alloy 625 in ASTM D1141-98 artificial seawater (Table 1) deaerated with 99.999% Ar were generated. The test solution was created using the ASTM D1141-98 parameters for a 2L sample size.

Table 1: Composition of ASTM D1141-98 artificial seawater used for polarization curves. Solution pH = 8.2

Compound	Concentration (g/L)
NaCl	24.53
$MgCl_2$	5.20
Na_2SO_4	4.09
$CaCl_2$	1.16
KCl	0.695
$NaHCO_3$	0.201
KBr	0.101
H_3BO_3	0.027
$SrCl_2$	0.0025
NaF	0.003
H_2O	988.968

Open circuit potential (OCP) and cyclic polarization (CPP) measurements were conducted on a lollipop shaped sample (Figure 1) of Alloy 625. The sample was wet polished with 400, 600, 800, 1200, and 2000 SiC grit and cleaned with deionized water and ethanol then air dried.

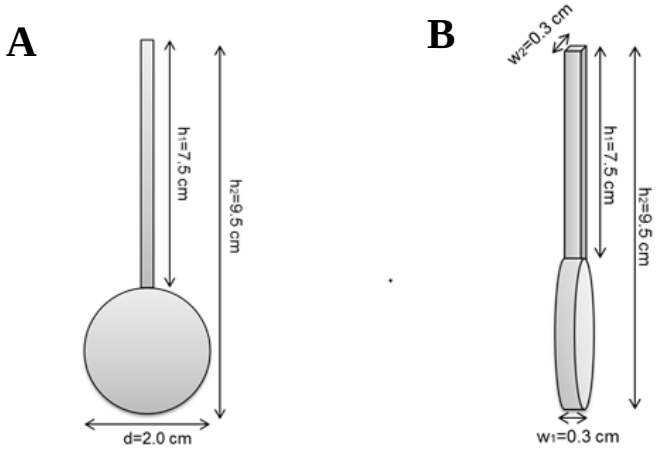

Figure 1: A. Front view Alloy 625 sample geometry and dimensions for deaerated seawater polarization test. **B.** Side view Alloy 625 sample geometry and dimensions for deaerated seawater polarization test.

Testing was conducted using a Gamry Reference 600 Potentiostat. The working electrode in the experiment was the lollipop Alloy 625 sample; the reference electrode was a saturated calomel electrode (SCE); the counter electrode was a niobium coated platinum mesh. The complete laboratory setup of the deaeration cell is shown in Figure 2. The deaerated artificial seawater (DASW) solution was deaerated for 1 hour prior to testing.

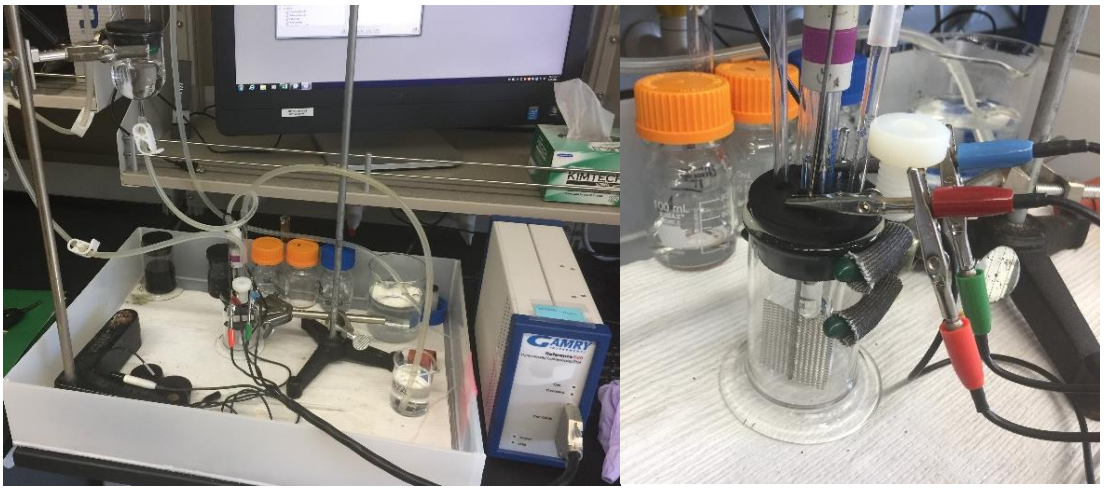

Figure 2: Experimental setup of the deaerated seawater OCP and CPP testing.

Steady state OCP was monitored for 1 hour with a cathodic polarization potential of -0.3V_{SCE} applied for 1 minute (to remove any oxygen in solution) before CPP began. All parameters were kept in accordance with previous experiments run for 3.0m, 3.5m, 4.0m, and 5.0m solutions [4] and the ASTM G61 standard [5]. Initial Gamry parameters are in Table 2.

Table 2: Parameters used in Gamry Reference 600 to conduct cyclic polarization experiment.

Initial Potential, E_i	-0.02 V_{OCP}
Maximum Potential, E_{Apex}	1 V_{Ref}
Final Potential, E_f	0 V_{OCP}

Maximum Current Density, I_{Apex}	100 mA/cm^2
Scan Rate (forward and reverse)	0.6 V/h

After the experimental data was collected, all values were converted to a standard hydrogen electrode (SHE) for input into COMSOL. All future potential references are to SHE.

COMPUTATIONAL METHODS

The COMSOL model framework for this case was the iron in acetic acid experiment conducted by J.C. Walton [6] and subsequent tutorial for the modeling software. This tutorial was modified further by Stenta [7] and Muñoz-Miller [4] to incorporate Alloy 625 and ASTM artificial seawater experimental data. Stenta's model focused on the dissolution of a single metal species, whereas the current model setup was designed in regards to the simulated critical crevice solution for Alloy 625 in a one dimensional crevice (Table 3). The base models were run using a 3.0m polarization curve as Muñoz-Miller [4] determined this to be the CCS for Alloy 625.

Table 3: Average wt% of Nb, Mo, and Cr, maximum wt% of Fe, and balance Ni in Alloy 625

Element	wt%	Molecular Weight (g/mol)
Nb	3.65	92.906
Mo	9.00	91.907
Fe	5.00	55.845
Cr	21.50	51.996
Ni	60.85	57.930

Because the tutorial [6] and previous modeling [7] used a pure metal as the corroding element, a variation to the model was required for the stoichiometric dissolution of Alloy 625. The equivalent charge, n_j, for Alloy 625 was determined using Equation 1:

Equation 1

$$n_j = \sum \left(\frac{mol_i}{mol_{total}} \right) * n_i$$

Where n_i is the charge per species. For this model, Fe had a +2 charge, Cr had a +3 charge, Nb had a +5 charge, Mo had a +3 charge, and Ni had a +2 charge. For Alloy 625, an equivalent charge of 2.3722 was determined. The equivalent charge of the alloy is required to calculate the flux of species i at the metal-solution interface, N_i (Equation 2):

$$N_i = \sum_{j=1}^{j_{max}} \frac{\nu_{ij} i_j}{n_j F} \qquad \text{Equation 2}$$

Where ν_{ij} is the stoichiometric species i in reaction j, i_j is the current density from the polarization curve, and F is Faraday's constant. The transition state theory for reactions near equilibrium is utilized by COMSOL, meaning the reaction rates of the species are assumed to be "very fast" [6]. The total rate of reaction of species *i* in solution, R_i, is given by Equation 3:

$$R_i = \sum_{k=1}^{k_{max}} \left(-r_k \nu_{ik} \ln \left(\frac{\prod_{i=1}^{i_{max}} C_i^{\nu}{}_k}{K_k} \right) \right) \qquad \text{Equation 3}$$

Where r_k is the numerical rate parameter for reaction k, K_k is the equilibrium constant for reaction k, and the product of the concentration of species *i*. The calculation of flux and reaction rate are necessary in determining species concentration along the length of the crevice. The governing equations the COMSOL software processes in regards to mass transport, assuming a steady state reaction are:

$$\frac{\partial C_i}{\partial t} = 0 = D_i \frac{\partial^2 C_i}{\partial x^2} + \frac{z_i D_i F}{RT} \frac{\partial}{\partial x} \left(C_i \frac{\partial \phi_s}{\partial x} \right) + \frac{N_i}{nw} + R_i \qquad \text{Equation 4}$$

Where C_i is the initial concentration, x is the distance from the mouth of the crevice, z_i is the charge, D_i is the diffusion coefficient, R is the universal gas constant, T is the temperature, ϕ_s is

the solution potential, n is the stoichiometric coefficient of electrons, and w is the width of the crevice. As well, Equation 5 provides a modified Nernst-Planck equation [8] correlates the concentration gradient to current:

Equation 5

$$\frac{i}{nF} = -D_i \frac{dC_i}{dx}$$

The derivation of Equation 5 is available in Appendix A and would be in future work to verify the concentrations at various positions in the crevice based on current density. The mass transport equations must be bound by electroneutrality (Equation 6) since potential is an unknown variable.

$$\sum C_i z_i = 0$$

Equation 6

The equilibrium reactions and constants are provided in Appendix B and all initial parameters for the model coincide with the Muñoz-Miller model [4] unless explicitly stated in this report. The COMSOL model uses an initial guess at the points on the experimental polarization curve and then iterates until a converged solution for the specified applied potential (E_{app}) of $0.44V_{SHE}$ is reached. The model outputs the following results versus the position in the crevice: concentration, corrosion current density, and electrode potential.

DATA AND RESULTS

The experimental data collected was input into COMSOL and crevice corrosion models for varying polarization curves and varying gap sizes were constructed. The overall electroneutrality equation was manually added to the COMSOL report after the model was run for each case based on species concentration at $E_{app} = 0.44V_{SHE}$.

Polarization Curves

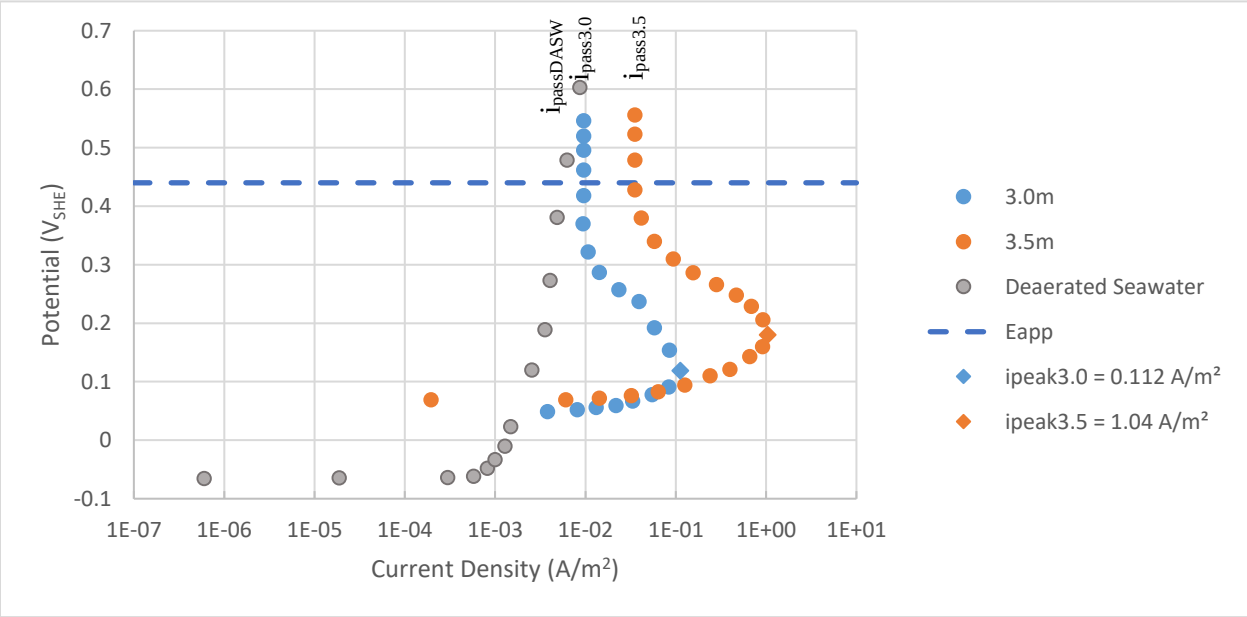

Figure 3: Experimental polarization curves input to COMSOL for calculations; curves were smoothed after $0.52V_{SHE}$. The deaerated seawater (DASW) experiment ran via the same process as the curves completed for the previously run 3.0m and 3.5m solutions (CCS for Alloy 625) [4].

COMSOL requires the polarization range to be constantly increasing or constantly decreasing. For the case of deaerated seawater, the range constantly increased from the lowest current density to the final point of analysis, $E_{app} = 0.44V_{SHE}$. The choice of end point for the polarization curve was determined based on the active to passive transition of the alloy [4]. Because COMSOL ended the model at $0.44V_{SHE,}$ the tail of the polarization curves were smoothed after 0.52V to avoid unnecessary computations.

From Figure 3, the corrosion potential (E_{corr}) for the DASW curve was $-0.0644V_{SHE}$, the peak current density (i_{peak}) was $6.27*10^{-3}A/m^2$ and was at the applied potential. The passive current density (i_{pass}) was taken at the applied potential as well and therefore equaled i_{peak}. For

the 3.0m polarization E_{corr} was 0.049V_{SHE}, i_{peak} was 0.112 A/m^2, and i_{pass} was 9.55*10^{-3}A/m^2. For the 3.5m polarization E_{corr} was 0.069V_{SHE}, i_{peak} was 1.04 A/m^2, and i_{pass} was 0.0352A/m^2.

Varying Gap Size

Crevice length (depth) remained constant for all models at 12.7mm [4], but crevice width was varied. Although all species reported in Appendix B were modelled, only the major metallic alloying cations, Na^+, Cl^-, H^+, and OH^- were illustrated to avoid graphical clutter. All specific species concentrations near the crevice tip, including compounds not visible in Figures 4 and 5, are tabulated in Table 4.

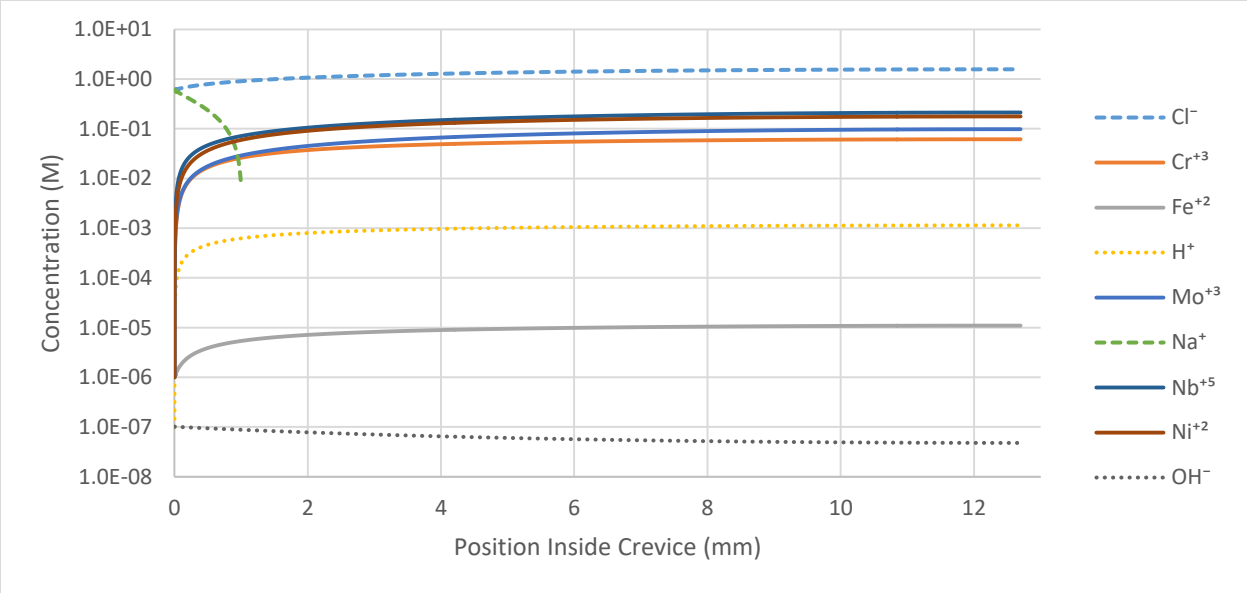

Figure 4: Concentration gradients for the proposed stoichiometric dissolution of Alloy 625 in ASTM D1141-98 artificial seawater (0.6M) using the 3.0m polarization curve. The position inside the crevice begins at 0mm (bulk solution) and ends at 12.7mm (tip). Crevice gap is 10µm and E_{app} = 0.44V_{SHE}.

In Figure 4, metallic cation (Fe^{+2}, Cr^{+3}, Ni^{+2}, Nb^{+5}, Mo^{+3}) concentration increased from essentially zero at the crevice mouth to concentrations on the order of 0.1M for species such as Ni^{+2} at the crevice tip. The dissolution of the major alloying elements of Alloy 625 illustrated active crevice propagation. It was also noted that the Na^+ concentration was only present near the crevice mouth. To maintain electroneutrality, the sodium ion could not migrate to the crevice tip with the higher concentrations of metallic cations present. However, the chloride

concentration increased from the bulk concentration (0.6M) to over 1M and the H^+ concentration increased by over four orders of magnitude from the bulk to the crevice tip.

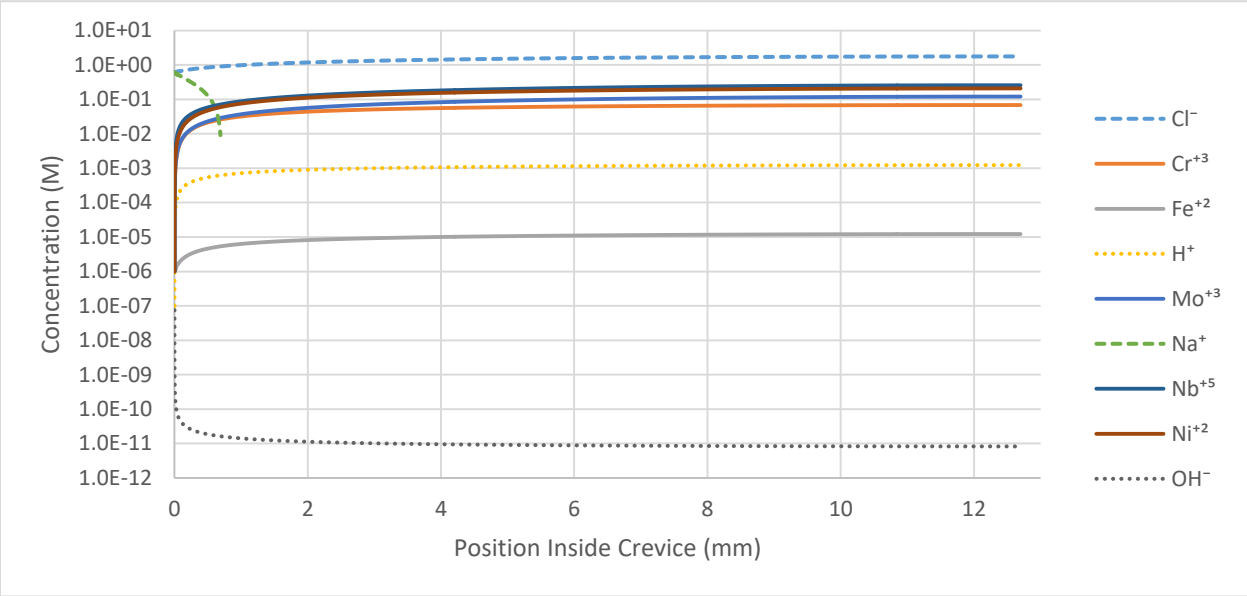

Figure 5: Concentration gradients for the proposed stoichiometric dissolution of Alloy 625 in ASTM D1141-98 artificial seawater (0.6M) using the 3.0m polarization curve. The position inside the crevice begins at 0mm (bulk solution) and ends at 12.7mm (tip). Crevice gap is 7µm and $E_{app} = 0.44V_{SHE}$.

In Figure 5, metallic cation (Fe^{+2}, Cr^{+3}, Ni^{+2}, Nb^{+5}, Mo^{+3}) concentration increased from essentially zero at the crevice mouth to concentrations on the order of 0.1M for species such as Ni^{+2} at the crevice tip, similar to the 10µm gap scenario demonstrated in Figure 4. To maintain electroneutrality, the sodium ion could not migrate to the crevice tip with the higher concentrations of metallic cations present. This happened closer to the crevice mouth for the 7µm gap. Cl^- and H^+ behavior was similar to the 10µm gap scenario.

The concentrations for the 7µm gap and 10µm gap were compared at an equal point in the crevice. Using COMSOL, the concentrations for the specified distance of 12.0mm were tabulated by the program from the 7µm gap and 10µm gap models (Table 4). The values were not reported for sodium since the ion was not present on the concentration profiles (Figures 4 and 5) near the tip of the crevice.

Table 4: Concentration of all modeled species for the 3.0m polarization curve as a function of crevice gap, C_{bulk0} = 0.6M, E_{app} = 0.44V_{SHE}, and a distance of 12.0mm from the crevice mouth.

Species	Concentration (M)	
	7 µm	**10 µm**
Cl^-	1.77	1.57
H^+	$1.23*10^{-3}$	$1.14*10^{-3}$
OH^-	$8.26*10^{-12}$	$4.79*10^{-8}$
Cr^{+3}	$6.83*10^{-2}$	$6.13*10^{-2}$
$CrOH^{+2}$	$8.82*10^{-3}$	$8.54*10^{-3}$
$CrCl^{+2}$	$3.31*10^{-1}$	$2.64*10^{-1}$
$CrCl_3$	$1.37*10^{-1}$	$8.55*10^{-2}$
Fe^{+2}	$1.22*10^{-5}$	$1.09*10^{-5}$
$FeCl_2$	$1.52*10^{-1}$	$1.07*10^{-1}$
Ni^{+2}	$2.07*10^{-1}$	$1.76*10^{-1}$
$NiOH^+$	$5.35*10^{-8}$	$4.90*10^{-8}$
$Ni(OH)_2$	$3.46*10^{-14}$	$3.42*10^{-14}$
$NiCl^+$	$7.79*10^{-1}$	$5.87*10^{-1}$
$NiCl_2$	$1.09*10^{-1}$	$7.30*10^{-2}$
Mo^{+3}	$1.20*10^{-1}$	$9.77*10^{-2}$
Nb^{+5}	$2.57*10^{-1}$	$2.12*10^{-1}$
Total Chloride	3.81	3.03

The only major difference in compound concentration between the 7µm gap and 10µm gap models was the hydroxide concentration. The total chloride for each case was calculated by adding together the concentrations of chloride in each relevant compound and multiplying it by its stoichiometric coefficient (i.e. the concentration of $FeCl_2$ was multiplied by two and added to the other species).

The model also reported the current density and potential along the length of the crevice (Figure 6A and 6B). These graphs were generated using the applied potential of 0.44V_{SHE}.

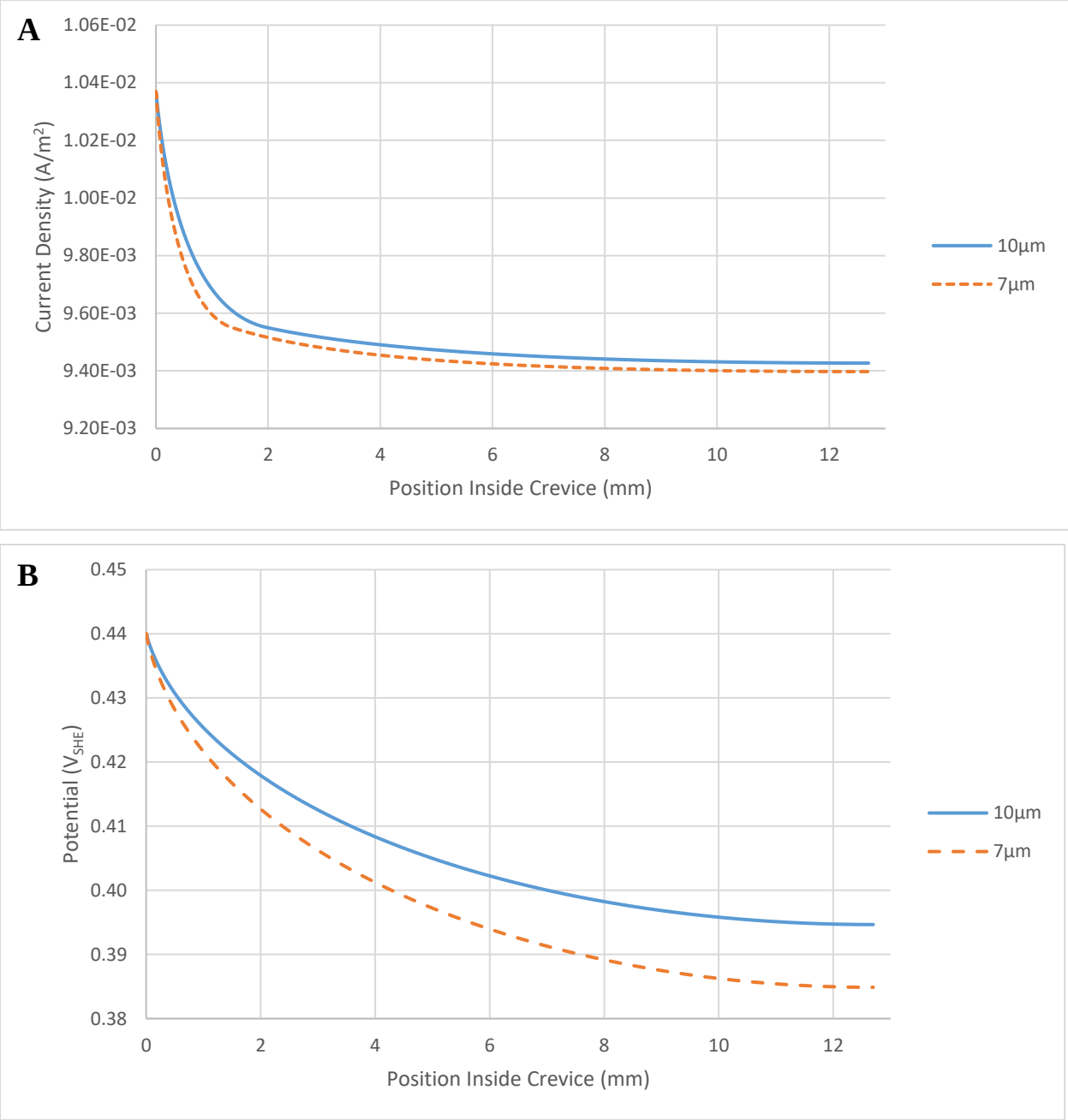

Figure 6: A. Corrosion current density versus position inside the crevice to compare a 10µm and 7µm crevice gap width with the 3.0m polarization curve, C_{bulk0} = 0.6M, E_{app} = 0.44V_{SHE}.

B. Potential versus position inside the crevice to compare a 10µm and 7µm crevice gap width with the 3.0m polarization curve, C_{bulk0} = 0.6M, E_{app} = 0.44V_{SHE}.

Dropping from the applied current of 0.44V_{SHE} at the crevice mouth, the potential drop flattened out as it approached the crevice tip (Figure 6B). The same phenomena occurred with the current

density (Figure 6A) as it reached a limit of approximately $9.40*10^{-3}$ A/m^2 for both crevice gap sizes, which is nearly i_{pass} for the 3.0m polarization curve.

The electroneutrality for both gap sizes was plotted by COMSOL for the applied potential of $0.44V_{SHE}$ (Figure 7). The minimal negative deviation from zero indicates an excess of positive charge present at the crevice tip for both gap sizes.

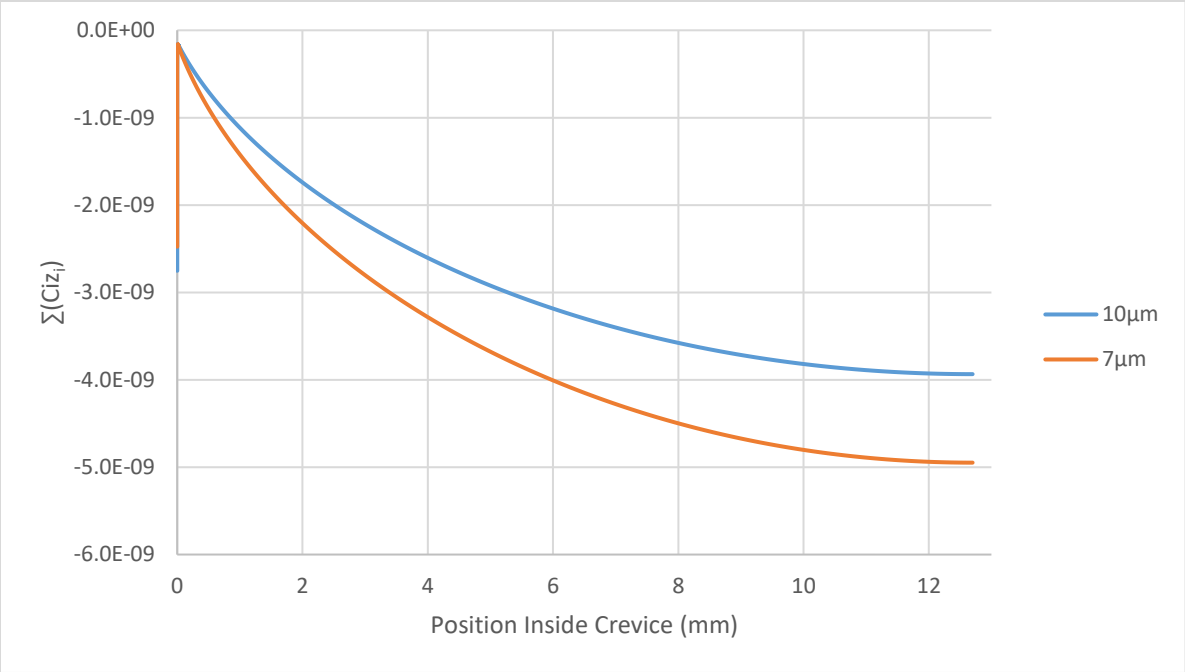

Figure 7: Electroneutrality versus position inside the crevice to compare a 10µm and 7µm crevice gap width with the 3.0m polarization curve, C_{bulk0} = 0.6M, E_{app} = $0.44V_{SHE}$.

Varying Polarization Curve

Crevice length (depth) and width (gap) remained constant for all models at 12.7mm [4] and 10µm, respectively, but the polarization curves were varied from 3.0m and 3.5m simulated CCS and DASW. This variance changed the potential and current values the model used to converge to the applied current of $0.44V_{SHE}$. Although all species reported in Appendix B were modelled, only the major metallic alloying cations, Na^{+}, Cl^{-}, H^{+}, and OH^{-} were illustrated to avoid graphical clutter. All specific species concentrations near the crevice tip, including compounds not visible in Figures 8 and 9, are tabulated in Table 5.

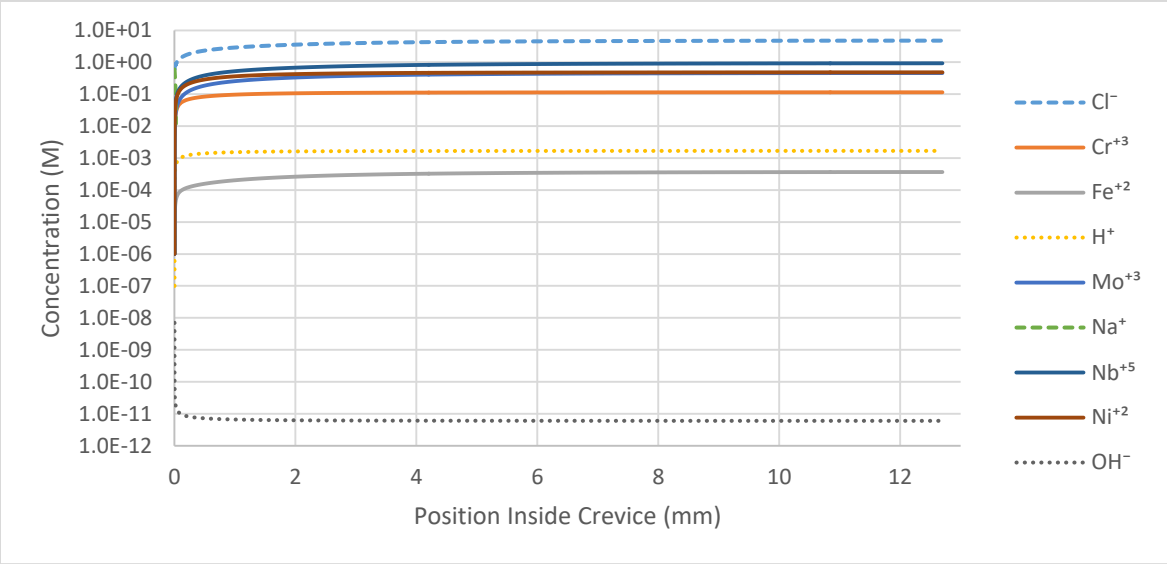

Figure 8: Concentration gradients for the proposed stoichiometric dissolution of Alloy 625 in ASTM D1141-98 artificial seawater (0.6M) using the 3.5m polarization curve. The position inside the crevice begins at 0mm (bulk solution) and ends at 12.7mmm (tip). Crevice gap is 10µm and $E_{app} = 0.44V_{SHE}$.

In Figure 8, metallic cation (Fe^{+2}, Cr^{+3}, Ni^{+2}, Nb^{+5}, Mo^{+3}) concentration increased from essentially zero at the crevice mouth to concentrations on the order of 0.5M for species such as Ni^{+2} at the crevice tip. This is higher than the 3.0m polarization curve metallic ion concentrations. The dissolution of the major alloying elements of Alloy 625 illustrated active crevice propagation. It was also noted that the Na^{+} concentration was only present at the crevice mouth. To maintain electroneutrality, the sodium ion could not migrate to the crevice tip with

the higher concentrations of metallic cations present. However, the chloride concentration increased from the bulk concentration (0.6M) to over 4M. The H^+ concentration increased by over four orders of magnitude from the bulk to the crevice tip and did so closer to the crevice mouth than the 3.0m polarization curve.

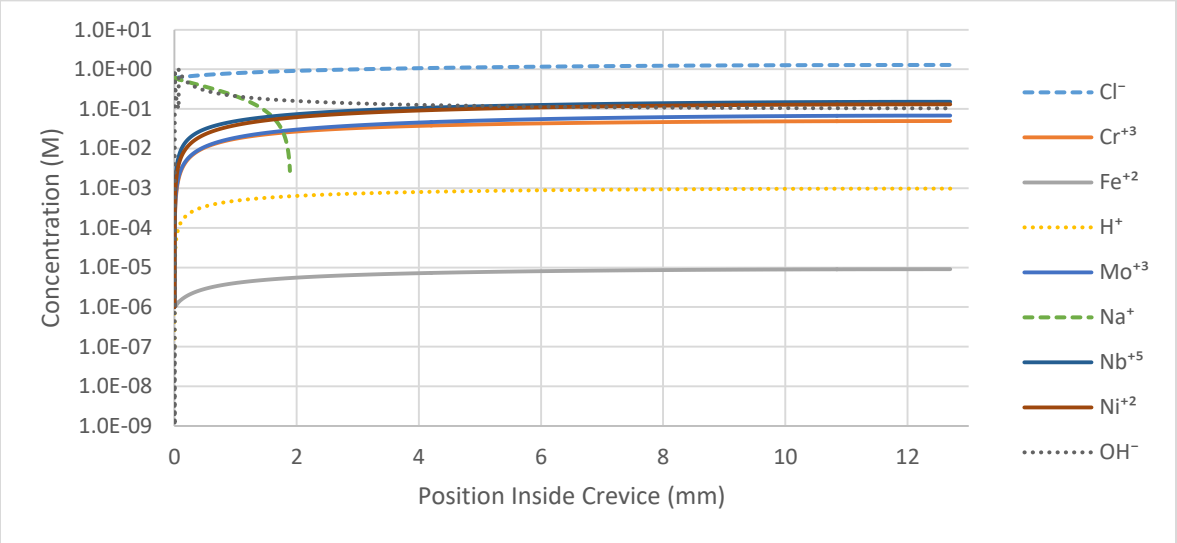

Figure 9: Concentration gradients for the proposed stoichiometric dissolution of Alloy 625 in ASTM D1141-98 artificial seawater (0.6M) using the DASW polarization curve. The position inside the crevice begins at 0mm (bulk solution) and ends at 12.7mmm (tip). Crevice gap is 10µm and $E_{app} = 0.44V_{SHE}$.

In Figure 9, metallic cation (Fe^{+2}, Cr^{+3}, Ni^{+2}, Nb^{+5}, Mo^{+3}) concentration increased from essentially zero at the crevice mouth to concentrations on the order of 0.1M for species such as Ni^{+2} at the crevice tip, similar to the 3.0m and 3.5m polarization curves. To maintain electroneutrality, the sodium ion could not migrate to the crevice tip with the higher concentrations of metallic cations present. However, the Na^+ did enter the crevice the greatest distance in this case. Cl^- and H^+ behavior was similar to the 3.0m gap scenario. However, the OH^- concentration was seven to eleven orders of magnitude higher at the crevice tip than the 3.0m and 3.5m polarization curve models. This excess negative charge at the crevice tip could account for the migration of positive sodium ions further along the length of the crevice than the previous cases.

The concentrations for the 3.0m, 3.5m, and DASW polarization curves were compared at an equal point in the crevice. Using COMSOL, the concentrations for the specified distance of 12.0mm were tabulated by the program (Table 5). The values were not reported for sodium since the ion was not present on the concentration profiles (Figures 4, 8, and 9) near the tip of the crevice.

Table 5: Concentration of all modeled species for the 10μm gap as a function of polarization curve, C_{bulk0} = 0.6M, E_{app} = 0.44V_{SHE}, and a distance of 12.0mm from the crevice mouth.

Species	Concentration (M)		
	3.0m	**3.5m**	**DASW**
Cl^-	1.57	4.74	1.29
H^+	$1.14*10^{-3}$	$1.69*10^{-3}$	$9.76*10^{-4}$
OH^-	$4.79*10^{-8}$	$6.01*10^{-12}$	$1.04*10^{-1}$
Cr^{+3}	$6.13*10^{-2}$	$1.15*10^{-1}$	$4.95*10^{-2}$
$CrOH^{+2}$	$8.54*10^{-3}$	$1.08*10^{-2}$	$8.04*10^{-3}$
$CrCl^{+2}$	$2.64*10^{-1}$	1.50	$1.75*10^{-1}$
$CrCl_3$	$8.55*10^{-2}$	4.44	$3.84*10^{-2}$
Fe^{+2}	$1.09*10^{-5}$	$3.67*10^{-4}$	$9.03*10^{-6}$
$FeCl_2$	$1.07*10^{-1}$	3.28	$5.96*10^{-2}$
Ni^{+2}	$1.76*10^{-1}$	$4.84*10^{-1}$	$1.31*10^{-1}$
$NiOH^+$	$4.90*10^{-8}$	$9.07*10^{-8}$	$3.45*10^{-14}$
$Ni(OH)_2$	$3.42*10^{-14}$	$4.27*10^{-14}$	$3.58*10^{-1}$
$NiCl^+$	$5.87*10^{-1}$	4.88	$3.66*10^{-2}$
$NiCl_2$	$7.30*10^{-2}$	1.83	$4.23*10^{-8}$
Mo^{+3}	$9.77*10^{-2}$	$4.59*10^{-1}$	$6.79*10^{-2}$
Nb^{+5}	$2.12*10^{-1}$	$9.26*10^{-1}$	$1.52*10^{-1}$
Total Chloride	3.03	34.67	1.73

Again, the major difference between the 3.0m, 3.5m, and DASW polarization curves was the hydroxide concentration and the nickel hydroxide compounds. As well, the chloride containing compounds and free chloride concentrations were significantly higher for the 3.5m polarization curve.

The model also reported the current density and potential along the length of the

crevice (Figure 10A and 10B). These graphs were generated using the applied potential of $0.44V_{SHE}$.

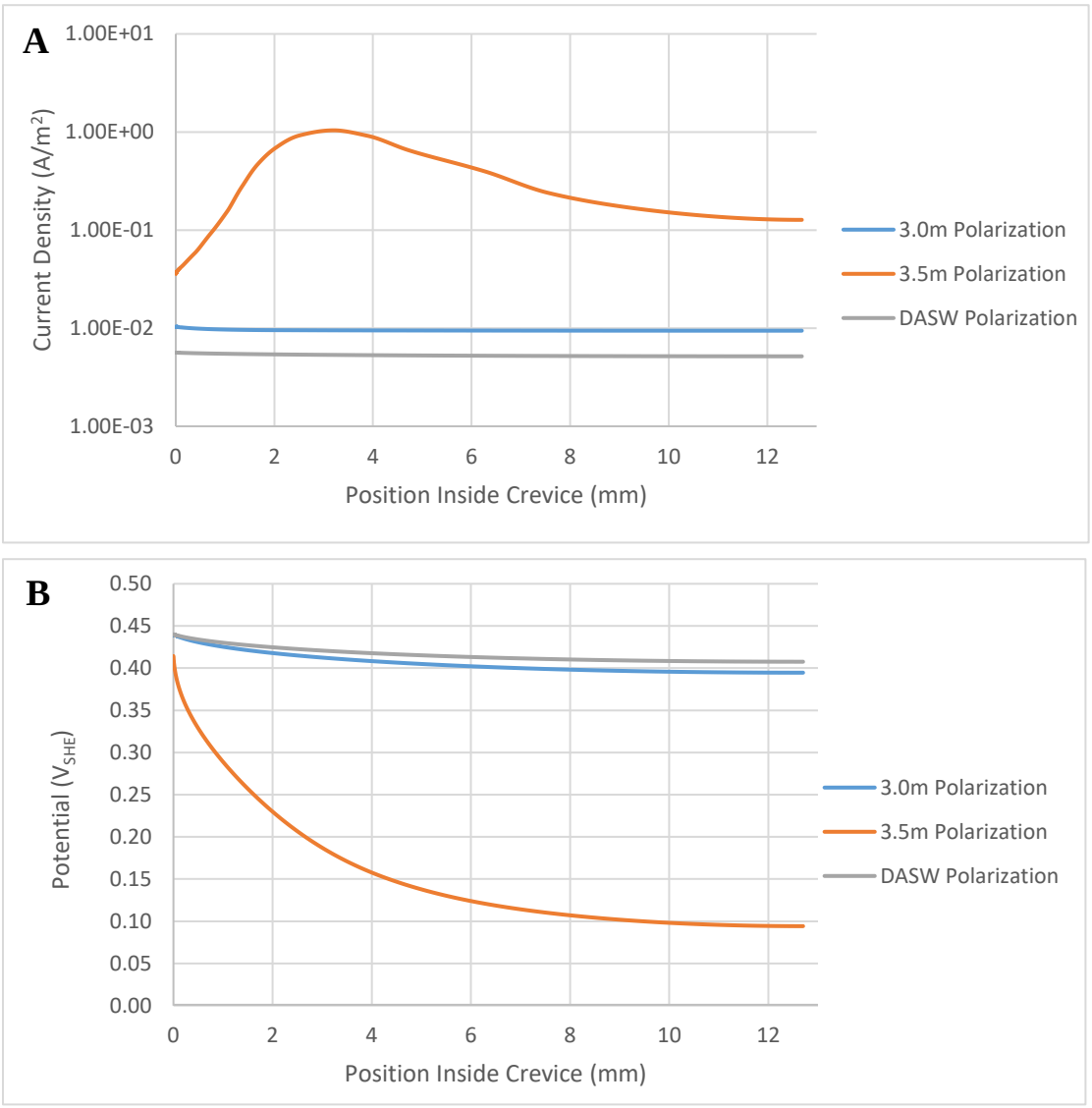

Figure 10: A. Corrosion current density versus position inside the crevice to compare 3.0m, 3.5m, and DASW polarizations with a 10µm gap, C_{bulk0} = 0.6M, E_{app} = $0.44V_{SHE}$.

B. Potential versus position inside the crevice to compare 3.0m, 3.5m, and DASW polarizations with a 10µm gap, C_{bulk0} = 0.6M, E_{app} = $0.44V_{SHE}$.

A polynomial fit was added to the 3.5m and DASW polarization curves for use in future modeling with the modified Nernst-Planck equation (Equation 5). The line of best fit for 3.5m is $y=6E+13x^6 - 2E+12x^5 + 3E+10x^4 - 2E+08x^3 + 626325x^2 - 254.24x + 0.0463$ $R^2=0.9737$. The line of best fit for DASW is $y=4.4679x^2 - 0.088x + 0.0056$ $R^2=0.9826$.

Dropping from the applied current of $0.44V_{SHE}$ at the crevice mouth, the potential drop flattened out as it approached the crevice tip (Figure 10B). A larger potential drop was present for the 3.5m polarization curve. The current density for the 3.0m and DASW polarizations remained relatively constant along the length of the crevice (Figure 10A). Aside from having an initial higher current, the 3.5m polarization reached a peak current density two orders of magnitude higher than the 3.0m and DASW polarization curves near the crevice mouth.

The electroneutrality for all three polarization curve models was plotted by COMSOL for the applied potential of $0.44V_{SHE}$ (Figure 11). The minimal negative deviation from zero indicates an excess of positive charge present at the crevice tip.

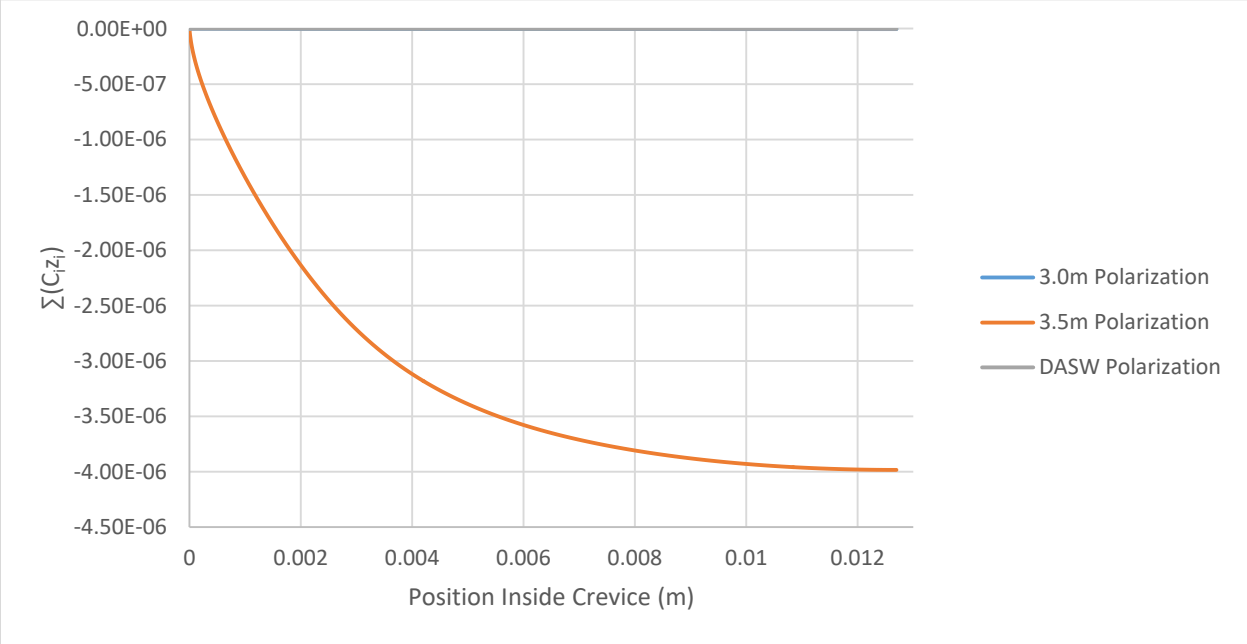

Figure 11: Electroneutrality versus position inside the crevice to compare 3.0m, 3.5m, and DASW polarizations with a 10µm gap, C_{bulk0} = 0.6M, E_{app} = $0.44V_{SHE}$. The 3.0m and DASW lines are on the order of 10^{-9} and therefore appear as zero on the figure above.

DISCUSSION AND ANALYSIS

Concentrations

Convergence of the model over the entire range of potentials (Figure 3) proved to be the limiting factor in success of the case studies. Models were attempted for a 4.0m polarization curve, but could not converge after the peak current density of approximately 1 A/m^2 and electroneutrality could not be held to approximately zero (Figures 7 and 11). As well, convergence could only be achieved with the current species reactions (Appendix B) if the equilibrium constants for $FeCl^+$ and $FeCl_2(s)$ were manually altered by 10^{-4}. Systematic variation of the equilibrium constants proved that the model could only maintain a balanced charge in the crevice with the aforementioned change. In comparison, literature values for these ferrous chloride equilibrium constants range from 1.16 to 2.59 [4, 9, 10].

Based on the concentrations from Tables 4 and 5, the concentration of chloride ions was very high in respect to all the other species. Sodium ions were seen dropping off in concentration close to the mouth of the crevice and this was expected due to the model's boundary conditions (Equation 6) to hold electroneutrality along the crevice length [6]. With higher concentrations of the metal cations due to the dissolution of Alloy 625, sodium ions were forced from the tip of the crevice. The chloride concentration in the crevice appeared high to balance the positive charge of the metallic cations and metallic hydroxides. When the chlorides reacted with iron, they were no longer providing this balance and for this reason, the equilibrium constant for the ferrous chlorides had to be decreased. From Tables 4 and 5, the free chloride concentration within the crevice varied from 1.29M with the DASW polarization curve to 4.74M with the 3.5m polarization curve; free chloride concentration was similar between the varied crevice gaps. However, the incredibly high total chloride concentration (34.7M) for the 3.5m

polarization curve was likely due to the formation of precipitation products ($CrCl_3$(s), $FeCl_2$(s), and $NiCl_2$(s)).

Varying Gap Size

Oldfield and Sutton [1,2] note the importance of the gap to depth ratio for crevices. The pair noted that narrower gaps resulted in ideal conditions for the CCS to occur and permanently break down any protective passive film on the alloy. The resistance in the gap, R, is found using Equation 7:

$$R = \frac{l\rho}{A} \qquad \text{Equation 7}$$

Where l is the length of the crevice, ρ is the solution resistivity, and A is the area of the crevice. For the purpose of this one dimensional model, the area was defined as the crevice length (12.7mm) multiplied by the crevice gap (7μm or 10μm). A smaller crevice gap resulted in a lower area and therefore a higher resistance. This resistance was then related to the potential drop in the crevice by Equation 8:

$$V = IR \qquad \text{Equation 8}$$

Figure 6 compares a crevice gap of 10μm with a crevice gap of 7μm using a 3.0m polarization curve. The 10μm gap had an IR drop of approximately 46mV while the 7μm gap had an IR drop of approximately 56mV. This IR drop should cause the metal within the crevice to maintain a potential in the active region of the anodic polarization curve [3, 11].

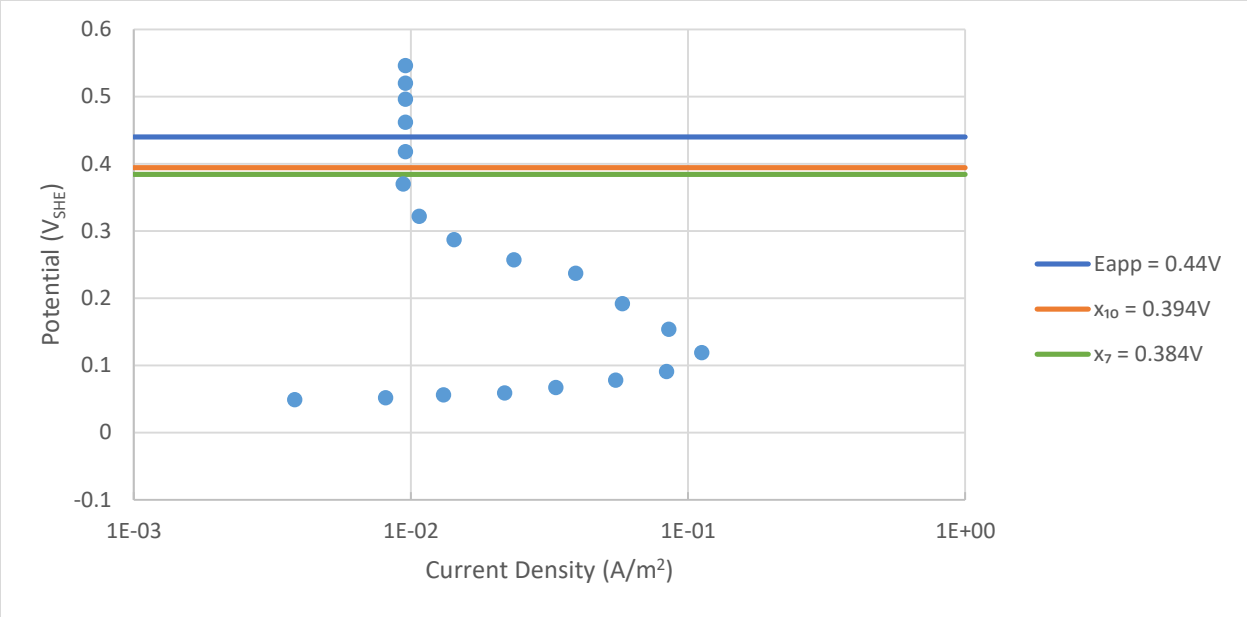

Figure 12: Polarization curve of 3.0m solution. E_{app} = 0.44V and x_{10} is the potential drop for the 10µm crevice at the crevice tip and x_7 is the potential drop for the 7µm crevice.

However, from Figure 12 above, even though the potential for the smaller crevice gap size was approaching the active nose of the curve, it had not yet crossed into the active dissolution portion which began at approximately 0.295V_{SHE}. Continuing to minimize the crevice gap resulted in a deviation from electroneutrality (Figure 8) and the models could not be verified and therefore were not included.

Varying Polarization Curves

Comparison of polarization curves for 3.0m, 3.5m and DASW, all with a crevice gap of 10µm, and all other variables held constant, were shown in Figure 10. There was little difference in corrosion current density or potential along the length of the crevice for the 3.0m and DASW models. The IR drop for 3.0m with a 10µm gap was shown in Figure 12 (x_{10}) and the DASW was comparable in that neither entered the active dissolution region of the curve. However, there

was a large IR drop for the 3.5m solution of approximately 346mV and a varying corrosion current density with a peak near the mouth of the crevice (Figure 13).

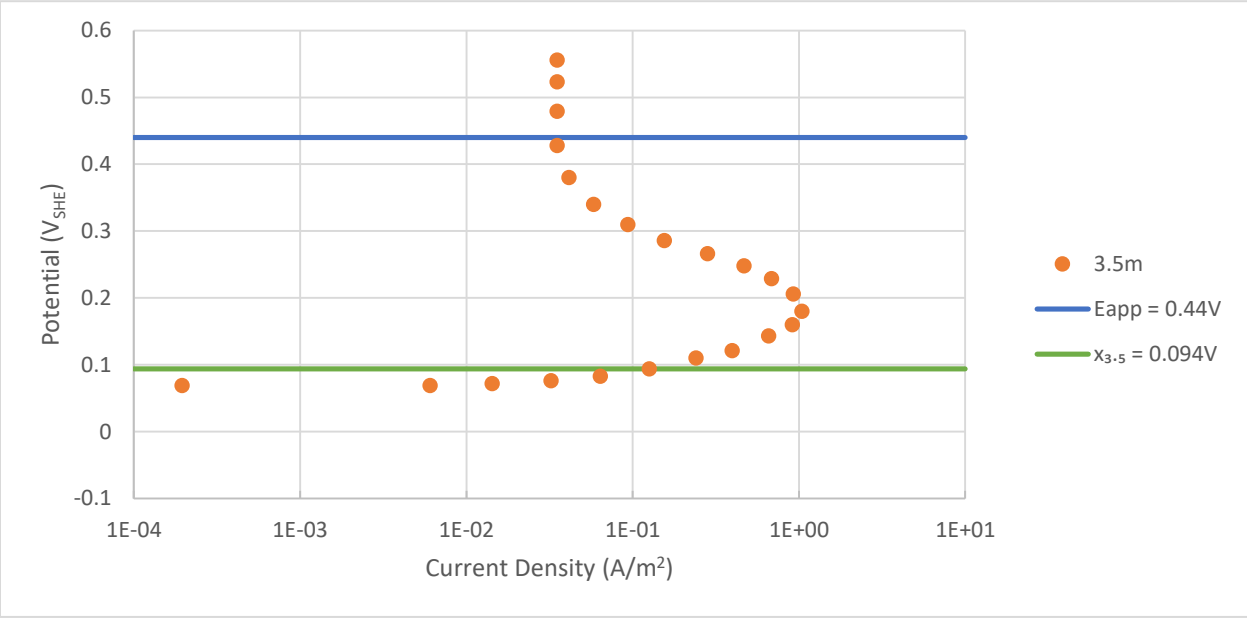

Figure 13: Polarization curve of 3.5m solution. E_{app} = 0.44V and $x_{3.5m}$ is the potential drop for the 10µm crevice at the crevice tip.

As mentioned previously for the varying crevice sizes, large IR drop caused the metal within the crevice to maintain a potential in the active region of the anodic polarization curve [3, 11]. However, as opposed to crevice geometry, the current density input to Equation 2 was different for the 3.5m polarization curve as compared to the 3.0m curve. Which subsequently changed the concentrations (Figure 8) determined through mass transport (Equation 4) and varied the corrosion in the crevice [6]. The disparity in peak current densities, nearly three orders of magnitude, from the polarization curves of DASW and 3.5m are testament to the role that formation of a CCS has on the propagation of crevice corrosion.

CONCLUSIONS

COMSOL Model

The current model set up can provide limited insight into the crevice propagation of Alloy 625 in 3.0m and 3.5m simulated CCS and DASW with a crevice gap of 10μm and 7μm. The three stage model of crevice corrosion proposed by Oldfield and Sutton [1,2] is confirmed from the COMSOL models. First, there was no oxygen present in the critical crevice solutions and DASW used for the polarization curve data, nor is oxygen present in the initial model parameters. Second, the H^+ concentration rose by at least four orders of magnitude in each model, thus lowering the pH of the system. To satisfy the third criteria, corrosion was occurring within the simulated crevices, as the concentation of the metallic ions of the major elements of Alloy 625 increased along the length of the crevice.

The high IR drop based on crevice geometry and CCS proposed by Shaw et. al [3] is achievable in the model using higher peak current densities (3.5m CCS polarization curve) to maintain active dissolution in the crevice. The difference in peak current densities from the 3.5m to the 3.0m polarization curve is 0.982A/m^2, Δi_{pass} is 0.0257 A/m^2, and this resulted in an IR drop difference of 300mV. However, the effect of IR on the propagation of crevice corrosion is less clear in the model's current state based on its inability to converge at crevice gaps smaller than 7μm and polarization curve data for simulated CCS greater than 3.5m.

Cost and Safety

The 2016 NACE study of Corrosion Costs and Preventative Strategies in the United States places the direct cost of corrosion at $451 billion or 2.7% of the US GDP annually [12]. Crevice corrosion directly affects many industries, but in particular transportation [4], and has an annual cost of over $29.7 billion in the US [13]. As well as ships and aircraft, crevice corrosion

was found to be the initial fault in the infamous Silver Bridge collapse in Gallipolis, Ohio resulting in the death of 46 travelers in 1967. A fundamental design flaw left the eyebar chain joint predisposed to form crevices. The crevice environment in the joint could not be detected using any normal inspection methods and a 3mm crack formed and ultimately led to catastrophic failure, millions of dollars in damage, loss of life, and sweeping legislation changes [14]. As of 2017, corrosion prevention and monitoring related jobs directly employed 2% of Ohio's workforce [15]. The complex problem of crevice corrosion, and all other forms of corrosion, are directly affecting the livelihood of American citizens. Through further modeling breakthroughs, design flaws and crevice environments will be better understood.

RECOMMENDATIONS

Although the COMSOL model converged for the aforementioned Alloy 625 cases, there are several cases currently where it will not converge: 4.0m and 5.0m simulated CCS polarization curves [4]. As well, the assumed ferrous chloride equilibrium constants do not compare to literature which deserves further examination. Future model enhancements:

- Reducing the model to a single element and systematically adding reactions if convergence is achieved. It is possible the precipitation reactions are hindering convergence.
- Verifying diffusion coefficients and equilibrium constants as the model is rebuilt
- Varying crevice pH from 7 [1, 11]
- Varying crevice gap to depth ratio [1, 2]
- Two-dimensional crevice geometry

Once the model is convergent with these improvements and electroneutrality is maintained, previous experimental work [4, 7] gives data for a known current at a known position in the crevice. This will enhance model focus to highlight the modified Nernst-Planck Equation (Appendix A) from an input of current versus position in addition to the working model which solves the Nernst-Planck equation using an experimental polarization curve (potential versus current). This manipulation will give a more accurate portrayal of crevice corrosion propagation.

ACKNOWLEDGMENT

The investigator gratefully acknowledges the previous work conducted by Dr. Aaron Stenta and Dr. Diana Muñoz-Miller. As well, the continued support of Dr. R. S. Lillard as the direct sponsor of this report.

REFERENCES

[1] J. W. Oldfield and W. H. Sutton, *British Corrosion Journal,* Vol. 13 (1), p 13-22, 1978.

[2] J. W. Oldfield and W. H. Sutton, *British Corrosion Journal,* Vol. 13 (3), p 104-111, 1978.

[3] B. A. Shaw, P. J. Moran, and P. O. Gartland, *Corrosion Science,* Vol. 32 (7), p 707-719, 1991.

[4] D. Muñoz-Miller, *University of Akron Ph.D Qualifying Exam,* 2016.

[5] ASTM Standard G61, "Test Method for Conducting Cyclic Potentiodynamic Polarization Measurements for Localized Corrosion Susceptibility of Iron-, Nickel, or Cobalt-Based Alloys" (West Conshococken, PA: ASTM, 2014).

[6] J.C Walton, *Corrosion Science,* Vol. 30 (8, 9), p. 915–928, 1990.

[7] A. Stenta, et. al, *NACE CORROSION,* Vol. 72 (11), p. 1328-1341, 2016.

[8] G. T. Gaudet, et. al, *AIChE Journal,* Vol. 32 (6), p. 949-958, 1986.

[9] M. S. Lee, *Metals and Materials International,* Vol. 10 (4), p. 387-392, 2004.

[10] D. K. Nordstrom, et. al, *American Chemical Society,* p. 399-413, 1989.

[11] R. S. Lillard and J. R. Scully, *J. Electrochem. Soc.,* Vol. 141 (11), p. 3006-3015, 1994.

[12] "International Measure of Prevention, Application, and Economics of Corrosion Technologies Study," *NACE International,* 2016.

[13] "Corrosion Costs and Preventative Strategies in the United States," *NACE International,* 2002.

[14] A. G. Lichtenstein, *J. Performance of Construction Facilities,* Vol. 7 (4), p. 249-261, 1993.

[15] "Economics of the Corrosion Industry: State of Ohio Report," *NACE International,* 2017.

APPENDIX A – Derivation of Nernst-Einstein and Sample Calculation

Derivation

$$\frac{i}{nF} = -D_i \frac{dC_i}{dx}$$

$$idx = -D_i nF dC_i$$

$$\int_0^x idx = -\int_{C_0}^{C_i} D_i nF dC_i$$

$$-\frac{1}{D_i nF}\int_0^x idx = C_i - C_0$$

3.5m Polarization

$$-\frac{1}{D_i nF}\int_0^x 6 * 10^{13}\mathrm{x}^6 - 2 * 10^{12}\mathrm{x}^5 + 3 * 10^{10}\mathrm{x}^4 - 2 * 10^{8}\mathrm{x}^3 + 626325\mathrm{x}^2 - 254.24\mathrm{x} + 0.0463dx = C_i - C_0$$

$$-\frac{1}{D_i nF}\left(8.57 * 10^{12}x^7 - 3.33 * 10^{11}\mathrm{x}^6 + 6 * 10^{9}\mathrm{x}^5 - 5 * 10^{7}\,\mathrm{x}^4 + 208775x^3 - 127.12x^2 + 0.0463x + 0.01037\frac{A}{cm^2}\right) = C_i - C_0$$

APPENDIX B – Equilibrium Reactions and Constants

Table 6: All input equilibrium reactions for each model case and their respective equilibrium constants

Reaction	Equilibrium Constant	Ref.
$H_2O \rightleftharpoons H^+ + OH^-$	$K_W = 1.01 \times 10^{-14}$	4
$Ni^{2+} + H_2O \rightleftharpoons Ni(OH)^+ + H^+$	$K_{Ni1} = 3.1623 \times 10^{-10}$	4
$Ni(OH)^+ + H_2O \rightleftharpoons Ni(OH)_{2,(aq)} + H^+$	$K_{Ni2} = 7.9433 \times 10^{-10}$	4
$Ni^{2+} + Cl^- \rightleftharpoons NiCl^+$	$K_{Ni3} = 2.1265$	4
$NiCl_{2,(s)} \rightleftharpoons Ni^{2+} + 2Cl^-$	$K_{Ni4} = 5.9237$	4
$Cr^{3+} + H_2O \rightleftharpoons Cr(OH)^{2+} + H^+$	$K_{Cr1} = 1.5849 \times 10^{-4}$	4
$Cr^{3+} + Cl^- \rightleftharpoons CrCl^{2+}$	$K_{Cr4} = 2.75$	4
$CrCl_{3,(s)} \rightleftharpoons Cr^{3+} + 3Cl^-$	$K_{Cr5} = 2.75$	4
$Fe^{2+} + H_2O \rightleftharpoons Fe(OH)^+ + H^+$	$K_{Fe1} = 5.0119 \times 10^{-9}$	4
$Fe(OH)^+ + H_2O \rightleftharpoons Fe(OH)_{2,(aq)} + H^+$	$K_{Fe2} = 7.9433 \times 10^{-12}$	4
$Fe^{2+} + Cl^- \rightleftharpoons FeCl^+$	$K_{Fe3} = 2.29 \times 10^{-4}$	Assumed
$FeCl_{2,(s)} \rightleftharpoons Fe^{2+} + 2Cl^-$	$K_{Fe4} = 2.51 \times 10^{-4}$	Assumed